Available online at www.sciencedirect.com
ScienceDirect
Journal of Power Sources 159 (2006) 1519–1526
JOURNAL OF POWER SOURCES
www.elsevier.com/locate/jpowsour

Polyaniline-based nickel electrodes for electrochemical supercapacitors—Influence of Triton X-100

T.C. Girija, M.V. Sangaranarayanan *

Department of Chemistry, Indian Institute of Technology, Madras 600 036, India

Received 6 October 2005; received in revised form 14 November 2005; accepted 16 November 2005
Available online 6 January 2006

Abstract

The influence of Triton X-100 in enhancing the capacitance of polyaniline-based nickel electrodes is reported. Cyclic voltammetric experiments, galvanostatic charge–discharge studies and impedance analysis were carried out in order to investigate the applicability of the system as an electrochemical supercapacitor. A qualitative interpretation of the enhancement is provided. Fourier transform infrared (FTIR), X-ray diffraction and scanning electron microscopy techniques were employed for characterization of the electrode.

Keywords: Cyclic voltammetry; Electrochemical supercapacitor; Impedance spectroscopy; Nickel; Polyaniline; Triton X-100

1. Introduction

The development of electrochemical supercapacitors for high-power applications constitutes a frontier area of research in the development of energy storage devices [1–4]. The origin of the high capacitance value arises from Faradaic pseudocapacitance as well as from adsorption phenomena. A large number of materials [5–7] such as carbon, transition metal oxides and electronically conducting polymers are under close scrutiny as electrode materials for supercapacitor applications. The origin of the high capacitance in the case of transition metal oxides and conducting polymers arises from the Faradaic reactions while for the carbon materials, it arises from the double layer at the electrode–electrolyte interface. Conducting polymers offer advantages [8,9] of lower cost in comparison with metal oxides and a higher charge density than carbon. These often have good intrinsic auto-conductivity and are inexpensive. Polyaniline (PANI) is unique among the family of conjugated polymers [10] since its doping level can be controlled in a facile manner, through an acid doping/base dedoping process. PANI possesses high conductivity, good redox reversibility, environmental stability [11] and has been extensively studied for diverse applications involving rechargeable batteries, electrochromic devices, sensors, etc. [12–16]. Nanostructured PANI offers the possibility of enhanced performance whenever higher interfacial area between PANI and its environment is essential [17]. In the design of supercapacitors requiring high surface area, nanostructured PANI should be an ideal candidate. Hence extensive attempts are being made to synthesize nanostructured PANI by addition of surfactants [18], polyelectrolytes [19], sulphonated dopants [20], etc. during polymerization.

Surfactants have important practical implications in wetting, formation of foams, etc. In addition to aggregation of surfactants at interfaces, aggregation of polymers at interfaces has also been studied [21]. Polymeric nanostructures are formed on surfaces due to a combination of interfacial, intra- and intermolecular forces [22]. The nonionic surfactant Triton X-100 (TX 100) is a commercial product obtained by ethoxylation of *p*-(1,1,3,3-tetramethylbutyl) phenol and contains ∼9.5 oxyethylene units per molecule [23]. There are several theoretical

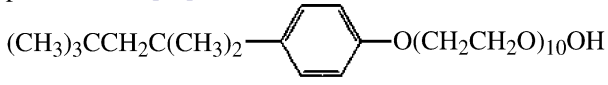

Structure of TX 100

[24,25] and experimental [26] studies concerning micellar properties of the TX 100 system. Nonionic surfactants are employed for suppressing the polarographic maxima in polarography [27] and for accelerating the ion transfer across polarized

* Corresponding author. Tel.: +91 44 22574209; fax: +91 44 22570545.
E-mail address: sangara@iitm.ac.in (M.V. Sangaranarayanan).

0378-7753/$ – see front matter © 2005 Published by Elsevier B.V.
doi:10.1016/j.jpowsour.2005.11.078

water/oil interfaces [28]. Nonionic surfactants are preferable to ionic surfactants in the polymerization of PANI. For example, although the anionic surfactants would enhance the solubility and the stability of the PANI, the emulsion requires a high molar ratio of the surfactant since one part of the surfactant acts as a dopant while the other part stabilizes the reactive medium. On the other hand, nonionic surfactants offer decreased sensitivity [29] of the latex to acidity and ionic strength. Further, their surface activity can be adjusted by changing the length of hydrophile–lipophile ratio and they are more compatible with a variety of polymers. Nonionic surfactants are known to be less sensitive to pH than their ionic counterparts and thus their ability to stabilize the PANI water-borne polymerization process should be better.

In the present study, PANI is electrochemically synthesized by potentiodynamic deposition on nickel in the presence of a nonionic surfactant, Triton X-100 (TX 100). The presence of the nanostructured material is inferred from scanning electron microscopy (SEM) studies. A specific capacitance value of $\sim 2.30 \times 10^3\ \mathrm{F\,g^{-1}}$ is deduced using impedance spectroscopy and galvanostatic charge–discharge studies.

2. Experimental

Analar grade aniline (SRL Ltd., India) was vacuum-distilled at 120 °C before use. Analar grade $HClO_4$, $NaClO_4$ and Triton X-100 (SRL Ltd., India) were used as received. Double-distilled water was used for the preparation of solutions. Electrochemical measurements were made in a one-compartment cell with a three-electrode configuration using a commercially available Ni foil of 1 cm^2 area as the working electrode, Ag/AgCl (Bio Analytical Systems, USA) as the reference electrode, while Pt wire (Bio Analytical Systems, USA) served as the counter electrode. The electrolyte solution for electropolymerization consisted of 0.1 M aniline, 0.1 M $HClO_4$ and 3 M $NaClO_4$ and various concentrations of TX 100 (0.2, 2, 5, 10, 20, 30 and 50 mM). The deposition of PANI was carried out potentiodynamically wherein the working electrode was subjected to potential cycling between −0.2 and 1.2 V versus Ag/AgCl at a scan rate of $300\ \mathrm{mV\,s^{-1}}$ for 100 cycles. After deposition, the coated polyaniline films were rinsed with 0.1 M $HClO_4$ and 3 M $NaClO_4$ in order to remove soluble monomeric species. Cyclic voltammetry, galvanostatic charge/discharge experiments and impedance analysis were performed using an electrochemical workstation CHI 660A (CH Instruments, USA). The impedance measurements were recorded in the frequency range 100 kHz to 10 mHz with an excitation signal of 5 mV. All the experiments were carried out at a temperature of 32 ± 1 °C. Scanning electron microscopy (SEM) images were recorded using JEOL JSM-840A instrument. X-ray diffraction pattern of the sample was recorded using a Shimadzu XD-D1 powder X-ray diffractometer using Cu Kα source. The Fourier transform infrared (FTIR) spectra of PANI was recorded on a Perkin Elmer FT-IR spectrophotometer from KBr pellets.

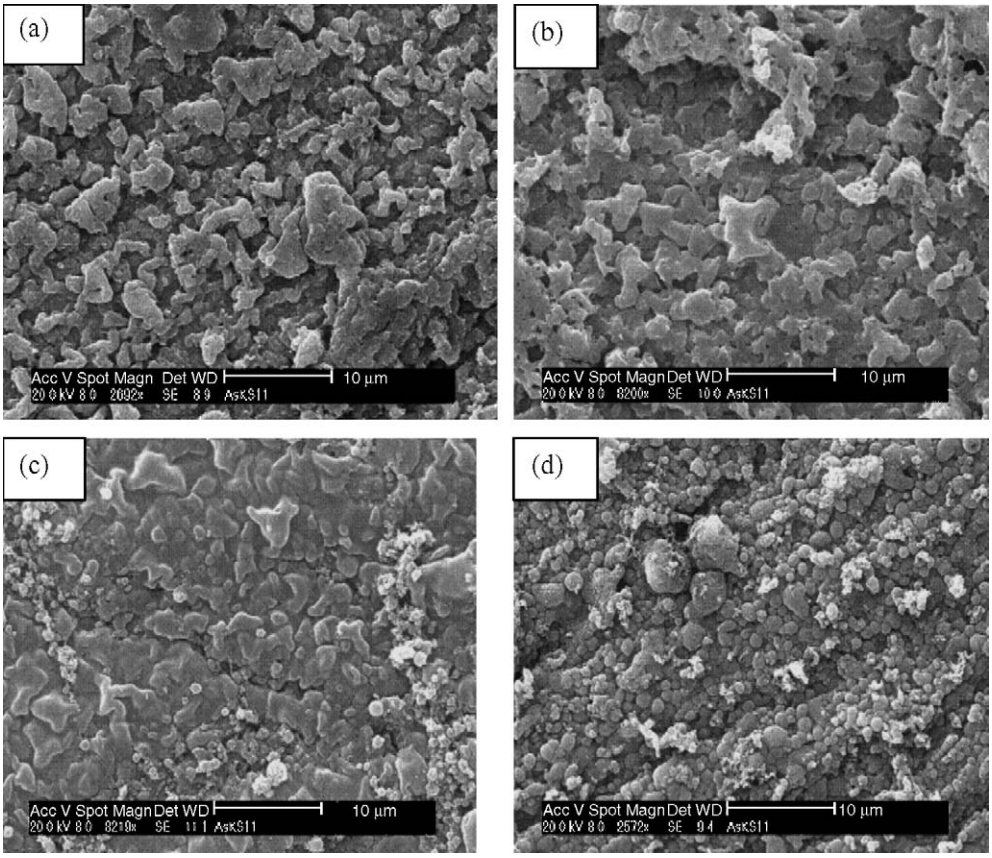

Fig. 1. Scanning electron micrographs of PANI deposited potentiodynamically on Ni foil in the presence of various concentrations of TX 100: (a) 0 mM, (b) 0.2 mM, (c) 2 mM and (d) 20 mM.

3. Results and discussion

3.1. SEM characterization

Fig. 1 depicts the SEM images of the PANI formed potentiodynamically on Ni substrate in the presence of various concentrations of TX 100. It is seen from Fig. 1a that the PANI film formed in the absence of TX 100 has a porous and layered structure. Fig. 1b and c depict the PANI film formed in the presence of 0.2 and 2 mM TX 100 concentration. In these cases, the morphology of PANI is not changed substantially. However, at concentration of 20 mM TX 100 (Fig. 1d), smooth PANI films having particle sizes of ~200 nm are formed on Ni. Thus a highly nanostructured film of PANI is obtained in the presence of TX 100, at concentrations much higher than the critical micelle concentration of 0.3 mM [30].

3.2. X-ray diffraction analysis (XRD)

Fig. 2 depicts the XRD patterns of the Ni foil coated with PANI in the presence and absence of TX 100. Studies on XRD patterns of PANI are scarce in the literature [31,32]. The XRD pattern depicts reflections at 2θ values of 44.5° and 51.8°. On comparing with the JCPDF (Joint Committee Powder Diffraction Files) files, it is inferred that the two reflections correspond to either Ni metal or NiO, which is present beneath the PANI layer. Although no additional peaks have been noticed for PANI formed in the presence of TX 100, a two-fold increase in the peak intensity is inferred. In general, an enhancement of intensities of XRD peaks indicates a corresponding increase in crystallinity of the samples and in the case of PANI synthesized in the presence of surfactants such as dodecylbenzenesulphonic acid, sodium dodecyl sulphate, etc., XRD studies have demonstrated [33,34] that increase in intensity suggests a relatively ordered polymer film. The d-spacings and the relative intensities for the peaks for PANI synthesized in the presence of 20 mM TX 100 are given as 2.04, 1.77 and 1.25 Å, and 73.3, 100.0 and 40.0, respectively corresponding to the 2θ values of 44.5°, 51.8° and 76.3°.

3.3. FTIR studies

The FTIR spectrum of PANI in the presence and absence of TX 100 is shown in Fig. 3. The peaks observed at 3430 cm^{-1} are attributed to the N–H stretching vibrations. PANI films show C–N stretching frequencies in the range 1250–1300 cm^{-1} and the peak at 2925 cm^{-1} is attributed to the C–H stretching vibrations. There is little difference between the pattern of peaks observed for PANI films prepared in the presence and absence of TX 100 and no new peaks are observed indicating the absence of any significant interaction between TX 100 and aniline monomer.

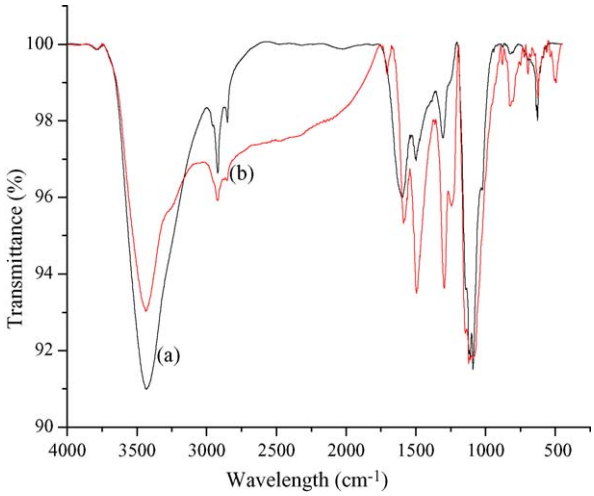

Fig. 3. FTIR spectra of PANI grown by potentiodynamic deposition on Ni substrate in the presence of (a) 0 mM TX 100 and (b) 20 mM TX 100.

3.4. Cyclic voltammetric studies

Fig. 4 depicts a typical voltammogram recorded for 100 continuous cycles during the polymerization of aniline on Ni substrate in the presence of 20 mM TX 100. The cathodic and anodic peak potentials at 0.1 and 1.0 V respectively have not been shifted appreciably from their corresponding positions in the cyclic voltammogram for electropolymerization in the absence of TX 100 implying that no complex formation between TX 100 and aniline has occurred. This feature has been inferred [35] in earlier investigations too; it has been demonstrated that the interaction of the polymer with the surfactant is not significant; in fact the surfactant upon adsorption on the Ni surface, alters the interfacial structure which facilitates the electropolymerization [36]. In the potentiodynamic method, a layer of PANI is deposited in

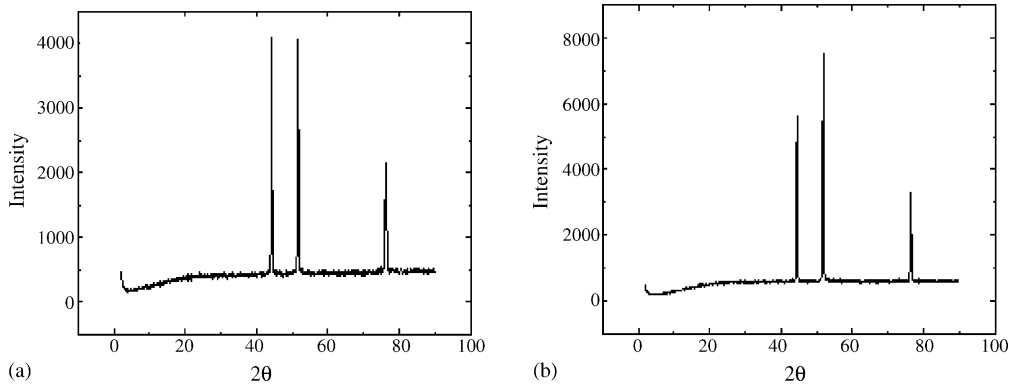

Fig. 2. X-ray diffraction spectra of PANI grown on Ni (a) absence and (b) presence of TX 100.

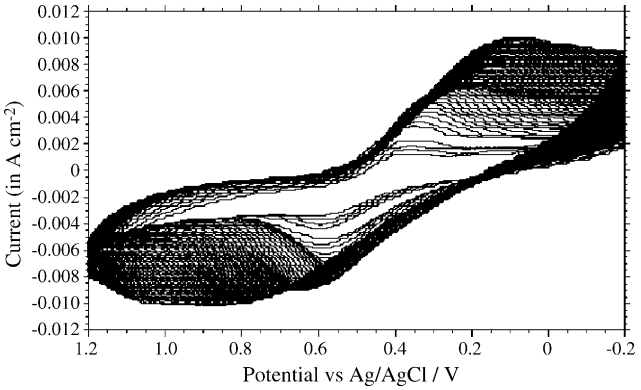

Fig. 4. Multi-cycle voltammogram depicting the electropolymerization of aniline on Ni from 0.1 M aniline + 20 mM TX 100 + 0.1 M $HClO_4$ + 3.0 M $NaClO_4$ at a scan rate of 300 mV s^{-1}. Number of cycles = 100.

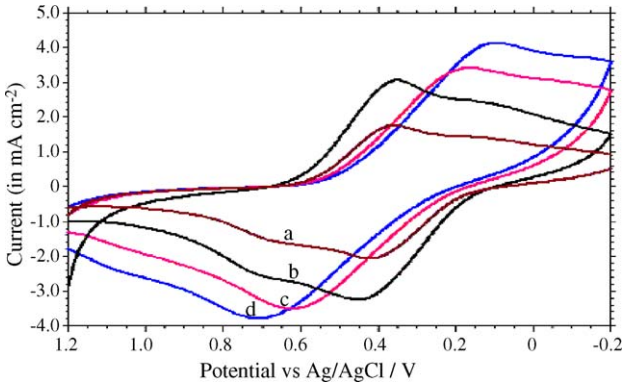

Fig. 6. Cyclic voltammogram for Ni/PANI (prepared in the presence of 20 mM TX 100) at various sweep rates: (a) 25.0 mV s^{-1}, (b) 50.0 mV s^{-1}, (c) 75.0 mV s^{-1} and (d) 100 mV s^{-1}.

each sweep between 0.9 and 1.2 V. In the potential range between −0.2 and 0.9 V, the deposited PANI undergoes reversible redox reactions, viz Leucoemeraldine/Emeraldine transition at 0.2 V and Emeraldine/Pernigraniline transition at 0.7 V. Thus the polymerization occurs layer by layer and each layer becomes electrochemically active before the next layer is deposited. Hence the PANI layers exhibit a pseudocapacitive behaviour. Thus the amount of PANI deposited also includes the charge consumed for pseudocapacitive behaviour due to the electrochemical activation of the PANI layer in the potential range of −0.2 and 0.9 V. This charge need not be excluded in the calculation of PANI deposited since the potential scanning is made between −0.2 and 1.2 V and also this electrochemical activation is a part of the formation of PANI by potentiodynamic method. Fig. 5 depicts the cyclic voltammogram (CV) for PANI electrode prepared in the presence and absence of TX 100. The area under the curve is markedly higher for the PANI electrode formed in the presence of TX 100 which implies an enhancement in the charge storage. Fig. 6 depicts the CVs of Ni/PANI electrode prepared in the presence of 20 mM TX 100 in 0.1 M $HClO_4$ + 3.0 M $NaClO_4$ at different scan rates. The cyclic voltammogram of the PANI-based electrode shows a pseudocapacitive current which arises mainly from the redox transitions of the PANI molecular chain. The dependence of voltammetric currents on the scan rate of CV is used to analyse the reversibility of electrode materials for supercapacitor applications. The linear dependence of the voltammetric currents on the scan rate indicates that the charge/discharge currents are typically capacitive-like.

3.5. Charge–discharge experiments

In order to further ascertain the feasibility of the Ni/PANI electrode material as a supercapacitor, galvanostatic charge–discharge cycles were constructed at current densities ranging from 1.5 to 4 mA cm^{-2}. A typical potential versus time profile for a constant current of 3.0 mA cm^{-2} is shown in Fig. 7. This behaviour is consistent with charging/discharging pattern (ideally a "ΛΛΛ…." shaped voltage response) exhibited by other supercapacitor electrode materials such as activated carbon, metal oxides, etc. in general [37]. Furthermore, the charge curves are symmetric to their corresponding discharge counterparts in the potential window indicating the practical feasibility of the PANI electrode in the presence of TX 100 for the development of supercapacitors. The pseudocapacitance can also be evaluated by charging–discharging responses via chronopotentiometry. The pseudocapacitance in this case is represented as [38]

$$C_{cp} = i\,\Delta t/\Delta v\,m \quad (1)$$

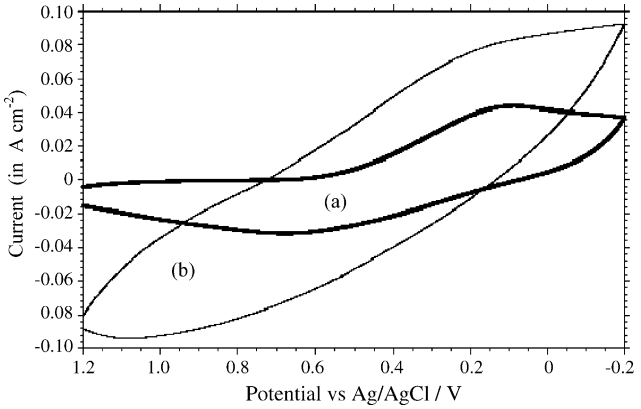

Fig. 5. Cyclic voltammogram for Ni/PANI prepared at (a) 0 mM TX 100 and (b) 20 mM TX 100 at a sweep rate of 300 mV s^{-1}.

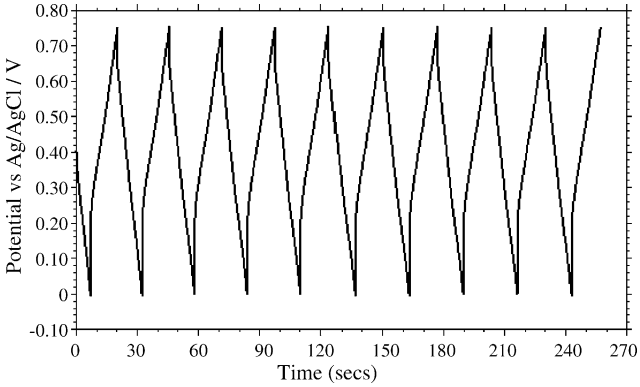

Fig. 7. Galvanostatic charge–discharge curves of Ni/PANI (TX 100) electrode at a current density of 3.0 mA cm^{-2}.

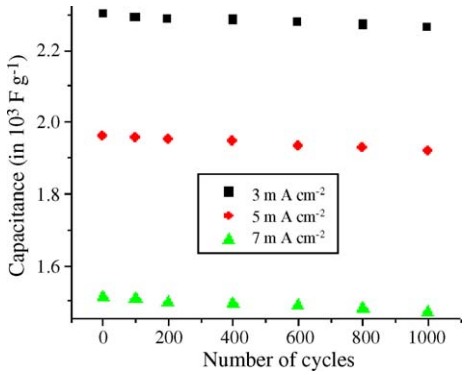

Fig. 8. Variation of capacitance with the number of cycles at various current densities.

where i, Δt, Δv and m denote respectively current density, discharge time, potential range and the active weight of the electrode material. Specific capacitances (F g^{-1}) of the order[1] of 2.30×10^3, 1.96×10^3 and 1.51×10^3 F g^{-1} are obtained at current values of 3.0, 5.0 and 7.0 mA cm^{-2} for an active weight of 0.014 mg cm^{-2} of PANI (estimated from the integration of the area under the anodic curve of the cyclic voltammogram of Fig. 4). The specific capacitance for PANI obtained in the absence of TX 100 is $\sim 1.28 \times 10^3$ F g^{-1}; hence an appreciable enhancement is obtained solely on account of the polymerization carried out in the presence of TX 100.

In order to evaluate the stability of the electrodes, the charge–discharge cycling tests were conducted for 1000 cycles. Fig. 8 shows the variation of specific capacitance with cycle number for Ni/PANI (TX 100) electrodes at various current densities. The specific capacitance of the Ni/PANI electrodes was as high as 2.30×10^3 F g^{-1} at the early stage of cycling for 3.0 mA cm^{-2} current density as seen from Fig. 8. However, the capacitance decreased to 2.27×10^3 F g^{-1} after 1000 cycles. This decrease in capacitance after 1000 cycles is consistent with the performance of other PANI based electrodes such as PANI/carbon [39], PANI/stainless steel [40] and $LiPF_6$ salt doped PANI [41].

3.6. Electrochemical impedance spectroscopy

Electrochemical impedance spectroscopy (EIS) was employed to obtain equivalent circuit parameters such as the charge transfer resistance and ohmic resistance, which enable mechanistic characterization of the system. Typical Nyquist diagrams for Ni/PANI electrode in 0.1 M $HClO_4$ + 3.0 M $NaClO_4$ solutions at different applied voltages (0.20–0.75 V) are given in Fig. 9. The impedance plots show a distorted semi-circle in the high-frequency region due to porosity of PANI and a vertically linear spike in the low-frequency region. The high-frequency intercept of the semi-circle on the real axis provides the value of ohmic resistance (R_Ω) and the diameter of the semi-circle gives an approximate value of the resistance (R_{ct}) of the PANI/electrolyte interface. Since the charge transfer resistance is the partial derivative of Faradaic current density (A cm^{-2}) with respect to the potential, R_{ct} has the units of Ω cm^2. The value of R_Ω is nearly invariant and is $\sim 4\,\Omega$ cm^2 for all the applied voltages. However, the value of R_{ct} increases with the applied voltage, which is deduced from the diameter of the semi circle. The angle made by low-frequency data on the real axis decreases on increasing the applied voltages of Ni/PANI electrode from 0.20 to 0.75 V. This trend is in agreement with the PANI formed on various substrates such as platinum [42] and stainless steel [40]. From the frequency (f^*) corresponding to the maximum of the imaginary component ($-Z''$) of the semi-circle, the time constant (τ) is calculated using the expression

$$\tau = 1/2\pi f^* \quad (2)$$

The value of τ obtained from Fig. 9 lies in the range of 0.001–0.1 s. Low values of τ are preferred for electrochemical capacitors in order to ensure fast charge/discharge characteristics [1]. The low-frequency capacitance (C_t) can be calculated from the variation of the imaginary component of the impedance with the reciprocal of the frequency ($-Z''$ versus $1/f$). The slope of this plot is equal to $1/2\pi C_t$ and for the potential range between 0.20 and 0.75 V, Z'' versus $1/f$ plots exhibit a linear correlation. The specific capacitance values (F g^{-1}) at various applied potentials of 0.20, 0.40 and 0.60 V are 2.45×10^3, 2.32×10^3 and 2.05×10^3, respectively. These values are consistent with that obtained from charge–discharge experiments (cf. Section 3.5). Fig. 10 depicts the equivalent circuit which is in accordance with the above Nyquist plot. In this model, the double layer capacity and the Warburg impedance for semi-infinite linear diffusion are replaced by two constant phase elements (CPEs). The two constant phase elements CPE_1 and CPE_2 correspond respectively to the double layer capacitance and diffusion process of the cations at the interface. In general, the appearance of a CPE may arise from (a) a distribution of the relaxation times as a result of diverse inhomogenities existing at the electrode/electrolyte interface, (b) porosity, (c) nature of the electrode and (d) dynamic disorder associated with diffusion. The proposed equivalent circuit for the Ni/PANI (TX 100) electrode can be compared with that of the Ni hexacyanoferrate composite electrode [43] wherein the cations from the electrolyte medium intercalate in and out of the electrode. It has been demonstrated [44,45] that polyaniline cation/perchlorate ion pair exhibit low solubility or dissociation, especially in comparison with the chloride and bisulphate ions. The fact that perchlorate ions are more strongly bound within the PANI film makes the expulsion of the anions more difficult in this case and hence the redox process occurs due to the diffusion of the H^+ ions present in the electrolyte through the polymer material. Hence the incorporation of the two CPE elements in the equivalent circuit corresponding to the porosity of the electrode and the semi-infinite diffusion of the ions become necessary. The fitting of the equivalent circuit was carried out using the AC impedance simulator of the electrochemical workstation and the parameters of the equivalent circuit are reported in Table 1. The impedances of the two constant phase elements

[1] The magnitude of specific capacitances contain three significant figures.

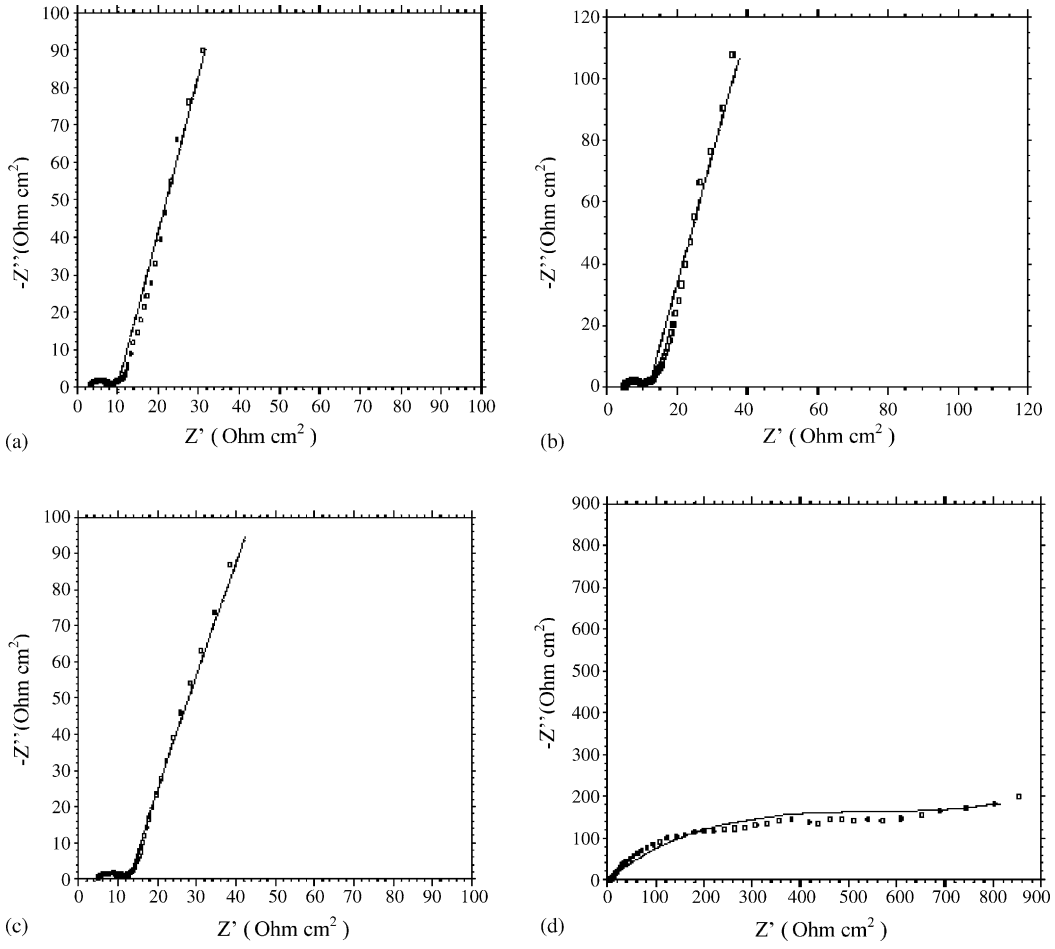

Fig. 9. Impedance spectrum in the frequency range 100 kHz to 10 mHz of Ni/PANI (TX 100) at various potentials: (a) 0.20 V, (b) 0.40 V, (c) 0.60 V and (d) 0.75 V. Squares denote experimental values while the line represents the fitting of the data to the equivalent circuit of Fig. 10 using the parameters of Table 1.

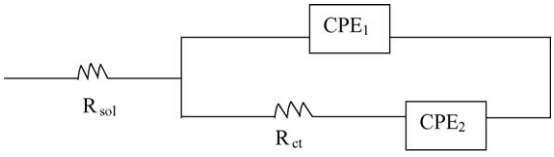

Fig. 10. Equivalent circuit for Ni/PANI (TX 100) electrode. R_{sol} is the electrolyte resistance, R_{ct} the charge transfer resistance, CPE_1 and CPE_2 denote constant phase elements.

are defined as [46,47] $Z_{CPE_1} = [Q(j\omega)^{n_1}]^{-1}$ and $Z_{CPE_2} = [Q(j\omega)^{n_2}]^{-1}$ with $-1 \leq n \leq 1$. While the constant value of Q is related to both the surface and the electroactive species, the exponent n arises from the slope of the $\log Z$ versus $\log f$ plot. n denotes the correction factor due to the roughness of the electrode with values ranging between 0 and 1. A pure capacitance yields $n = 1$, a pure resistance yields $n = 0$, while $n = 0.5$ represents Warburg impedance. From Table 1, it is inferred that within the potential window of 0.2–0.6 V (half-oxidized conducting emeraldine state) the value of n_1 ~0.7 implies the porous nature of the electrode and the value of n_2 (~0.9) indicates the highly capacitive nature of the system. At 0.75 V (completely oxidized state) $n_2 = 0.21$ depicts the resistive nature of the Ni/PANI electrode. The Nyquist plot obtained for PANI prepared in the absence and presence of various concentrations of TX 100 at an applied potential of 0.6 V is shown in Fig. 11. It is seen that the charge transfer resistance R_{ct} decreases with the increase of concentration of TX 100.

Table 1
Equivalent circuit parameters deduced by fitting the Nyquist plots

S. no.	Applied potential (V) vs. Ag/AgCl	R_{ct} (Ω cm^2)	CPE_1 (Ω^{-1} cm^{-2} s)	CPE_2 (Ω^{-1} cm^{-2} s)	n_1	n_2
1	0.2	5 ± 0.5	0.0025 ± 0.0005	0.088 ± 0.008	0.74 ± 0.05	0.90 ± 0.02
2	0.4	7 ± 0.2	0.001 ± 0.0002	0.08 ± 0.005	0.78 ± 0.02	0.85 ± 0.04
3	0.6	10 ± 1	0.004 ± 0.0001	0.075 ± 0.003	0.54 ± 0.04	0.84 ± 0.02
4	0.75	500 ± 2	0.00045 ± 0.00005	0.004 ± 0.0001	0.51 ± 0.01	0.21 ± 0.01

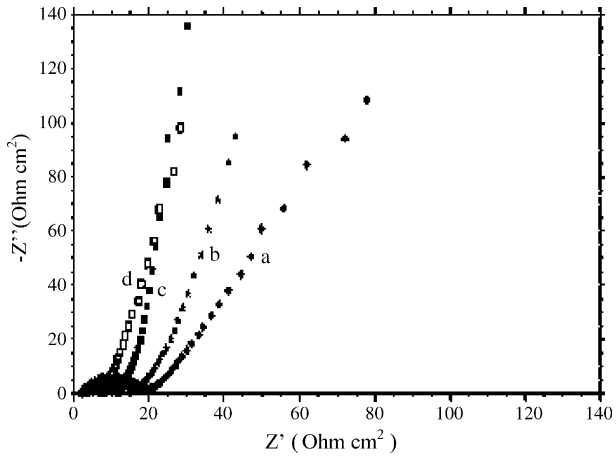

Fig. 11. Impedance spectrum in the frequency range 100 kHz to 10 mHz of Ni/PANI (TX 100) at various concentrations of TX 100: (a) 0 mM, (b) 5.0 mM, (c) 10.0 mM and (d) 20.0 mM at an applied voltage of 0.6 V.

3.7. Mechanism of the influence of TX 100

Surfactants are employed as additives in the polymerization processes in order to (i) affect the locus of polymerization using emulsion [48] or inverse emulsion [49] pathways, for altering the molecular and supramolecular structure of the resulting polymers and (ii) improve the conductivity, stability and processibility [50] of polymers.

In TX 100, there are no electrostatic interactions between the head groups of TX 100 and charged aniline at the hydrophilic interface of the micelles. For PANI prepared in the presence of TX 100 below the cmc (0.2 mM), there is no appreciable increase in capacitance (1.29×10^3 F g^{-1}) when compared with PANI prepared in the absence of TX 100 (1.27×10^3 F g^{-1}). Even more interesting is that for concentrations higher than cmc, viz 2, 5 and 10 mM, the respective capacitances are deduced as 1.44×10^3, 1.45×10^3 and 1.55×10^3 F g^{-1} not significantly different from 1.27×10^3 F g^{-1} reached in the absence of TX 100; however for 20 and 30 mM TX 100, the specific capacitance reaches a very high value of 2.30×10^3 F g^{-1} and 2.57×10^3 F g^{-1} (since the specific capacitance value at 50 mM concentration of TX 100, was not much different from that at 30 mM, concentrations higher than 50 mM were not employed in subsequent studies). Although the specific capacitance increases with the surfactant concentration in general, a marked enhancement is seen at a particular value viz 10 times the cmc. This implies that the morphology of PANI formed in the presence of TX 100 is dictated by the concentration of TX 100. Below cmc, there is no appreciable interaction between the neutral TX 100 and aniline monomer; hence no significant differences occur between the capacitance values in the presence and absence of TX 100. As the concentration becomes much higher than the cmc, polymerization is localized in the hydrophobic core of the micelle. Hence a compact and nanostructured polymer is produced thereby increasing the surface area of the PANI with enhanced adhesion to the Ni substrate – a consequence of the tendency of surfactants to reduce the interfacial surface tension. This results in the organized formation of the polymer on the Ni substrate. This inference is also supported by the XRD studies (cf. Section 3.2) wherein a highly crystalline nature has been deduced. At 20 mM concentration of TX 100, it is conjectured that marked structural changes of TX 100 micelles occur leading to a reinforced polymer network, which results in the unusually high specific capacitance of 2.30×10^3 F g^{-1} which is significantly higher than that of the PANI electrode synthesized without TX 100. For surfactant concentrations at and higher than 20 mM, the specific capacitance remains nearly a constant. In contrast, PANI synthesized in presence of *p*-toluene sulphonic acid on Ni electrodes has yielded [51] a value of $\sim 4.03 \times 10^2$ F g^{-1}, for specific capacitance.

The theoretical specific capacitance (C_{th}) of an electrode material is estimated in general, using the following equation [52]:

$$C_{th} = nF/\Delta VM \quad (3)$$

where n denotes the number of moles of charge transferred. F is the Faraday's constant and ΔV the potential window employed. C_{th} is deduced as 1.34×10^3 F g^{-1} since M equals 192.58 g mol^{-1} (the combined mass of aniline monomer and ClO_4^-) and $\Delta V = 0.75$ V. The specific capacitance of $\sim 1.30 \times 10^3$ F g^{-1} obtained in the absence of TX 100 correlates well with C_{th} estimated from the above equation. If interactions between aniline monomer and TX 100 were assumed leading to a complex polymer, then C_{th} would have decreased substantially to ~ 320 F g^{-1} since M in this case would become 839.58 g mol^{-1} and hence it is evident that the enhancement in capacitance can only be attributed to the morphology of PANI which has resulted from the localized polymerization of aniline in the presence of TX 100 and to the nanostructured nature of the film. It has also been previously shown [53] that TX 100 which bears a chain of approximately 10 ether groups, plays a crucial role in organizing the structure of the material and in creating well defined and reproducible nanophases wherein this group of surfactants participates in the formation and organization of clusters in solution. These high specific capacitances can be compared with those offered by other systems (1.74×10^3 F g^{-1}) such as nanocomposite material of $Ni(OH)_2$/ultrastable Y zeolites employing a template for the synthesis of $Ni(OH)_2$ and for PANI/stainless steel (0.80×10^3 F g^{-1}). The presence of TX 100 is known to give mechanical strength to the conducting polymer [54]. TX 100 has been employed previously to modify the properties of MnO_2 in alkaline storage batteries and was proved to be effective in enhancing the rechargeability characteristics. It has been demonstrated [55] that the addition of TX 100 yielded larger surface area, resulting in better discharge performance and lower degradation rate. In order to obtain the precise magnitude of specific capacitance for practical applications, two-electrode assemblies need to be fabricated.

4. Summary

The electropolymerization of aniline in the presence of Triton X-100 and perchloric acid media was carried out on nickel electrodes, in a potentiodynamic manner. The electrochemical

characterization of the polymer-coated nickel electrodes was carried out with the help of cyclic voltammetry, galvanostatic charge–discharge experiments and impedance spectroscopy. The estimated capacitance of $2.30 \times 10^3\,\mathrm{F\,g^{-1}}$ was shown to arise solely on account of the polymerization carried out in the presence of Triton X-100. FTIR, XRD and SEM studies were employed for characterization of the material. A plausible equivalent circuit was proposed and the corresponding circuit parameters were deduced for elucidation of the mechanism of charge transport.

Acknowledgement

The helpful comments of the reviewers are gratefully acknowledged. This work was supported by the DRDO, Government of India.

References

[1] A. Burke, J. Power Sources 91 (2000) 37.
[2] C. Lin, J.A. Ritter, B.N. Popov, J. Electrochem. Soc. 146 (1999) 3155.
[3] P. Soudan, J. Gaudet, D. Guay, D. Belanger, R. Schulz, Chem. Mater. 14 (2002) 1210.
[4] B.E. Conway, Electrochemical Supercapacitors: Scientific Fundamentals and Technological Applications, Kluwer Academic Publishers/Plenum Press, New York, 1999.
[5] S. Sarangapani, B.V. Tilak, C.P. Chen, J. Electrochem. Soc. 143 (1996) 3791.
[6] M. Hughes, G.Z. Chen, M.S.P. Shaffer, D.J. Fray, A.H. Windle, Chem. Mater. 14 (2002) 1610.
[7] F. Fusalba, H.A. Ho, L. Breau, D. Belanger, Chem. Mater. 12 (2000) 2581.
[8] A. Rudge, J. Davey, I. Raistrick, S. Gottesfeld, J.P. Ferraris, J. Power Sources 47 (1994) 89.
[9] A. Rudge, I. Raistrick, S. Gottesfeld, J.P. Ferraris, J. Power Sources 47 (1994) 89.
[10] W.S. Huang, B.D. Humphrey, A.G. MacDiarmid, J. Chem. Soc., Faraday Trans. 82 (1986) 2385.
[11] N. Oyama, T. Tatsuma, T. Sato, T. Sotomura, Nature 373 (1995) 598.
[12] W.A. Gazzoti, Facz, M.A. Depach, J. Electroanal. Chem. 415 (1996) 107.
[13] B.P. Jelle, G. Hagen, J. Electrochem. Soc. 140 (1993) 3560.
[14] C.D. Batich, H.A. Laitinen, H.C. Zhou, J. Electrochem. Soc. 137 (1990) 883.
[15] G. Inzelt, E. Csahok, V. Kertesz, Electrochim. Acta 46 (2001) 3955.
[16] G. Inzelt, M. Pineri, J.W. Schultze, M.A. Vorotyntsev, Electrochim. Acta 45 (2000) 2403.
[17] J. Huang, R.B. Kaner, J. Am. Chem. Soc. 126 (2004) 851.
[18] L. Yu, J.L. Lee, K.W. Shin, C.E. Park, R. Holze, J. Appl. Polym. Sci. 88 (2003) 1550.
[19] J.M. Liu, S.C. Yang, Chem. Commun. (1991) 1529.
[20] J. Yue, A.J. Epstein, J. Am. Chem. Soc. 112 (1990) 2800.
[21] D.W.C. Andrew, E.A. O' Rear, B.P. Grady, J. Am. Chem. Soc. 125 (2003) 14793.
[22] J.P. Rabe, Curr. Opin. Colloid Interf. Sci. 3 (1998) 27.
[23] A.N. Galatanu, I.S. Chronakis, D.F. Anghel, A. Khan, Langmuir 16 (2000) 4922.
[24] R.J. Robson, E.A. Dennis, J. Phys. Chem. 81 (1977) 1075.
[25] C. Tanford, Y. Nozaki, M.F. Rhode, J. Phys. Chem. 81 (1977) 1555.
[26] A.A. Ribeiro, E.A. Dennis, Biochemistry 14 (1975) 3746.
[27] J. Heyrovsky, P. Zuman, Practical Polarography, Academic Press, New York, 1968.
[28] Z. Yoshida, S. Kihara, J. Electroanal. Chem. 227 (1987) 171.
[29] N. Kohut-Svelko, S. Reynaud, J. Francois, Synth. Met. 150 (2005) 107.
[30] B. Factor, B. Muegge, S. Workman, Ed. Bolton, J. Bos, M.M. Richter, Anal. Chem. 73 (2001) 4621.
[31] A.G. MacDiarmid, A.J. Epstein, Science and Applications of Conducting Polymers, Adam Hilger, Bristol, 1991, p. 117.
[32] M.E. Jozefowicz, A.J. Epstein, J.P. Pouget, J.G. Masters, A. Ray, A. Sun, X. Tang, A.G. MacDiarmid, Synth. Met. 41–43 (1991) 723.
[33] D. Han, Y. Chu, L. Yang, Y. Liu, Z. Lv, Colloids Surf. A: Physicochem. Eng. Aspects 259 (2005) 179.
[34] X. Hu, K. Tang, S.-G. Liu, Y.-Y. Zhang, G.-L. Zou, React. Funct. Polym.
[35] T. Zalewska, A. Lisowska-Oleksiak, S. Biallozor, V. Jasulaitiene, Electrochim. Acta 45 (2000) 4031.
[36] R. John, M.J. John, G.G. Wallace, H. Zgao, in: R.A. Mackay, J. Tester (Eds.), Electrochemistry in Colloids and Dispersions, VCH Publishers, New York, 1992, p. 225.
[37] C.-C. Hu, C.-C. Wang, Electrochem. Commun. 4 (2002) 554.
[38] W.-C. Chen, T.-C. Wen, J. Power Sources 117 (2003) 273.
[39] W.-C. Chen, T.-C. Wen, H. Teng, Electrochim. Acta 48 (2003) 641.
[40] K. Rajendra Prasad, N. Munichandraiah, J. Power Sources 112 (2002) 443.
[41] K.S. Ryu, K.M. Kim, Y.J. Park, N.-G. Park, M.G. Kang, S.H. Chang, Solid State Ionics 152–153 (2002) 861.
[42] D. Belanger, X. Ren, J. Davey, F. Uribe, S. Gottesfeld, J. Electrochem. Soc. 147 (2000) 2923, references therein.
[43] U. Retter, A. Widmann, K. Siegler, H. Kahlert, J. Electroanal. Chem. 546 (2003) 87.
[44] R. Cordova, M.A. del Valle, A. Arratia, H. Gomez, R. Schrebler, J. Electroanal. Chem. 377 (1994) 75.
[45] M.C. Miras, C. Barbero, R. Kotz, O. Hass, J. Electroanal. Chem. 369 (1994) 193.
[46] J.R. Macdonald, Impedance Spectroscopy, Wiley, New York, 1987.
[47] J.O. Agak, R. Stoodley, U. Retter, D. Bizzotto, J. Electroanal. Chem. 562 (2004) 35.
[48] J.E. Osterholm, Y. Cao, F. Klavetter, P. Smith, Polymer 35 (1994) 2902.
[49] P. Swapna Rao, S. Subrahmanya, D.N. Sathyanarayana, Synth. Met. 128 (2002) 311.
[50] D. Han, Y. Chu, L. Yang, Y. Liu, Z. Lv, Colloids Surf. A: Physicochem. Eng. Aspects 259 (2005) 179.
[51] T.C. Girija, M.V. Sangaranarayanan, J. Power Sources 156 (2006) 705–711.
[52] L. Cao, L.B. Kong, Y. Liang, H. Li, Chem. Commun. (2004) 1646.
[53] O. Dag, I. Soten, O. Celic, S. Polarz, N. Coombs, G.A. Ozin, Adv. Funct. Mater. 13 (2003) 30.
[54] E.-L. Kupila, J. Kankara, Synth. Met. 55–57 (1993) 1402.
[55] M. Ghaemi, L. Khosravi-Fard, J. Neshati, J. Power Sources 141 (2005) 340.